The Abrasion of Photovoltaic Glass: A Comparison of the Effects of Natural and Artificial Aging

David C. Miller,[1] Asher Einhorn,[1] Clare L. Lanaghan,[1] Jimmy M. Newkirk,[1] Bobby To,[1] Derek Holsapple,[1] Joshua Morse,[1] Paul F. Ndione,[1] Helio R. Moutinho,[1] Aaesha Alnuaimi,[2] Jim J. John,[2] Lin J. Simpson,[1] Chaiwat Engtrakul[1]

[1]National Renewable Energy Laboratory (NREL), Golden, CO, 80401, USA

[2]Dubai Electricity and Water Authority (DEWA), Dubai, 564, United Arab Emirates

***Abstract* — Natural soiling and the subsequent requisite cleaning of photovoltaic (PV) modules result in abrasion damage to the cover glass. The durability of the front glass has important economic consequences, including determining the use of anti-reflective and/or anti-soiling coatings as well as the method and frequency of operational maintenance (cleaning). The abrasion of coatings and glass has been explored in a field study, including the soiling-prone locations of Dubai (United Arab Emirates), Kuwait City (Kuwait), Mesa (Arizona), Mumbai (India), and Sacramento (California). Dry-brush-cleaned specimens will be compared to those subjected to artificial-brush testing. The characteristics of material integrity, surface energy, optical transmittance, surface roughness, and scratch size were examined using an optical microscope, contact goniometer (for water), spectrophotometer, interferometer, and atomic force microscope (AFM), respectively. The findings of this study will be used to provide feedback regarding the cleaning equipment, cleaning methods, and coatings used in the PV industry. The study here will also be used to aid in developing an abrasion standard for the PV industry.**

***Index Terms* — abrasion, anti-reflective coating, anti-soiling coating, erosion, operations maintenance**

I. Introduction

Insolation, temperature, and contamination are the three primary natural factors affecting electricity generation in solar photovoltaic (PV) devices. Regarding the latter, natural soiling (contamination, including inorganic and organic matter) on the surface of PV modules can gradually reduce performance in the order of 1%·day^{-1} in the insolation-rich Middle East and North Africa (MENA) region, while sudden power drops as high as 70% have been recorded worldwide [1]. Strategies for improving performance by limiting soiling include coatings and cleaning. Anti-reflective (AR) and/or anti-soiling (AS) coatings may be added on the front glass to improve the throughput of incident light and/or to limit the accumulation of contamination. AR coatings gained popular use in the PV industry starting in ~2005, whereas AS coatings are presently being explored. A variety of manual and automated methods may be applied for the cleaning of PV modules, typically using a variety of equipment similar to that used in the building glazing industry. The weather conditions and corresponding field operating conditions for cleaning are, however, not standardized, e.g., daytime cleaning may be favored in some locations where manual cleaning is most extensively used, whereas thin film PV may be cleaned at night to prevent shading damage. Presently, there is concern about the longevity of AR and AS coatings, which may be subject to erosion damage during cleaning in addition to abrasion from airborne particulate matter. To provide technoeconomic benefit, the cost of a coating should justify its use if its lifetime is limited.

Representative glass coupon specimens are used in this study to examine the abrasion of PV first-surfaces, e.g., the surface of a module incident to direct solar radiation. Both field abrasion (resulting from airborne contamination and/or cleaning) and artificial abrasion (i.e., linear machine abrasion using a brush) have been investigated. The goals of this study include:

- Quantify the effect of abrasion on cover-glass performance, i.e., the optical transmittance.
- Quantify the abrasive typically present in challenging locations, i.e., the particle size distribution of the contamination.
- Characterize the damage morphology for specimens subject to initial field abrasion, i.e., the shape and size of scratches on specimens with as much as one year of weathering damage.
- Compare the damage morphology for field and artificial abrasion.
- Support the development of an abrasion test standard tailored to the PV industry.

II. Materials and Methods

2.1 Field-aged coupon specimens

The field aging of coupon specimens was previously described in Refs. [2] and [3]. Briefly, coupon specimens consist of coated substrates or substrates with no coating, 75 mm × 75 mm × 3.2 mm in size. Coated substrates were custom fabricated by industry suppliers to achieve the coupon size, which is smaller than a PV module. The coatings studied include AR and/or AS functionalities, which varied in surface energy (inFcluding hydrophilic and hydrophobic varieties). The coupons were mounted on black backplane in a custom fixture to achieve a daytime temperature similar to that of a PV module.

The specimens were weathered in or near the cities of Dubai, United Arab Emirates; Kuwait City, Kuwait; Mesa, Arizona;

Mumbai, India; and Sacramento, California. Each site was chosen to provide a soiling- and/or abrasion-prone location, combined with a meteorological climate of interest [2]. Specimens weathered for one year in Dubai—the most contamination-prone location in this study (a desert environment with frequent coastal dew cycles—will be used as a primary example.

A set of manual cleaning practices was performed to study the effects of abrasion and provide insights regarding soiling and the effectiveness of cleaning. Separate sets of all the coupon types were either: not cleaned (NC); cleaned with a horsehair-bristle dry brush (DB); cleaned with a low-pressure water spray (WS); or cleaned with a wet polypropylene sponge and rubber squeegee (WSS). Cleaning was repeated once each month. Two replicate specimens of each coupon type for each cleaning procedure were returned annually from all outdoor locations over five years.

2.2 Artificial machine abrasion

Artificial abrasion was performed using a linear brush tester (M/N 5060; BYK-Gardner GmbH). The 5060 tester was modified with a hopper that was mechanically triggered to dispense abrasive at the end of each brush cycle. Dry abrasive (A4 "coarse" AZ test dust [4]; Powder Technology Inc.) was used in the 5060 tester. Brushes with custom bristles (3.8-cm length; M.W. Jenkins' Sons Inc.) were used with the 5060 tester, including: polyamide (Nylon 6/12 copolymer), hog bristle, and polyester. 0, 500, 1000, 5000, 10000, 15000, and 20000 brush cycles (swiped both forward and reverse) were applied on separate coupons. The specimens were cleaned using non-contact methods (deionized water rinse, followed by clean dry air spray) after artificial abrasion. The glass- and phase-transition temperatures for the bristle materials were verified using differential scanning calorimetry (DSC) with a Q2000 instrument (TA Instruments, Inc.). The 2-Hz data was taken from the second of two consecutive cycles (from -100°C≤T≤250°C) at the rate of 10 °C·min^{-1} in a nitrogen environment (50 mL·min^{-1} purge). The diameter of the bristles was measured using a digital microscope (VHX-5000; Keyence Corp.). The base chemical composition of the bristles was analyzed using Fourier transform infrared (FTIR) spectroscopy with a commercial spectrometer (Nicolet Nexus 870, Thermo Fisher Scientific Inc.). Attenuated total reflectance (ATR) spectra were obtained from 4000 to 400 cm^{-1} in 4-cm^{-1} increments, using a 50-mm × 10-mm × 5-mm ZnSe crystal attachment (ATR Max-II, PIKE Technologies). The sampling depth of the FTIR measurements is estimated to be in the order of 2 μm for the specimens in this study.

2.3 Specimen characterization

Images of the abrasion and remaining contamination of the surface coatings were collected using the VHX-5000 microscope using at least five 1705-μm × 1278-μm images. Following Ref. [5], analysis of the contamination on the field-aged coupons was achieved using the ImageJ software (imagej.net) with custom scripts. The image-quality settings (brightness, contrast, texture, and color) were adjusted to provide increased contrast between the contamination and substrate surface. In order to grayscale the images for analysis, local thresholding was applied (Phansalkar method), followed by a fill operation (maximum radius of 5 μm). In this way, the particle area coverage (PAC) as well as the number and size of the contaminating particles could be quantified. The mass of the particles was estimated assuming a circular cross-sectional area profile, which was projected as an idealized spherical profile, with the density of 2.65 g·m^{-3} for silica. In comparison, Powder Technology Inc. (the AZ test dust vendor) uses a S3500 Laser Diffraction Particle Size Analysis Instrument (Microtrac Inc.) to quantify particle size distribution (PSD). Contact angles were measured using a "100–25–A" goniometer (Ramé-Hart Instrument Co.). Ten measurements were automatically performed using 4 μL of deionized water at three different locations within the same coupon. Optical performance was measured using a dual-beam ultraviolet-visible-near infrared (UV-VIS-NIR) spectrophotometer (Cary 5000; Agilent Technologies Inc.), in hemispherical transmittance (τ_h, with an integrating sphere, DRA-2500; Agilent Technologies Inc.) or in direct transmittance (τ_d, without an integrating sphere). A ~1-cm^2 sample area was locally examined with each optical measurement. The representative solar weighted transmittance [6] was determined for τ_h and τ_d to account for the photon flux on a single-junction PV device. A NT1100 (Wyko Corp.) scanning white-light interferometer was used to quantify the surface roughness of coupon specimens. The average of five separate regions on each specimen was examined using a 148-μm × 112-μm field of view. The surface of the coated glass samples was analyzed using an atomic force microscope (AFM; Dimension 3100; Bruker Corp.), operated in tapping mode using Nanoscope V electronics. The Dimension 3100 was used to characterize the depth, width, and frequency of scratches present on specimen surfaces. Separate measurements, 100 μm in width and ~33 μm in length, were obtained on five locations on each coupon examined. A WVASE 2000 (J.A Woollam & Co.) variable-angle spectroscopic ellipsometer was used to verify coating thickness on unaged specimens.

III. Results and Implications

3.1 Optical performance of the field coupon specimens

The enhancement of τ_h ("$\Delta\tau_h$ *for coating*" in Fig. 1) was determined from the difference between the measured τ_h of coated unaged specimens and the τ_h for the corresponding unaged glass substrate with no coating. In Ref. [3], a linear correlation was observed between PAC and τ_h in the sites examined allowing τ_h to be predicted ("*Predicted* $\Delta\tau_h$" in Fig. 1) from the measured PAC of the soiled field coupon specimens. The change in τ_h ("*Actual* $\Delta\tau_h$" in Fig. 1) was then quantified from the field specimens relative to the measured τ_h

for unaged specimens. The *Predicted* $\Delta\tau_h$, *Actual* $\Delta\tau_h$, and their *Difference* are shown in Fig. 1 for DB cleaned specimens after 1 year in Dubai. The variation of measurement for the *Actual* $\Delta\tau_h$ for three regions within the same specimen is shown in Fig. 1 for 1 S.D. A similar *Predicted* $\Delta\tau_h$ is observed for specimens B, D, E, J, and U, based on the similar PAC present on the DB cleaned specimens. The least *Difference* between *Predicted* $\Delta\tau_h$ and *Actual* $\Delta\tau_h$ is observed in Fig. 1 for materials J (glass with no coating) and U (polymer anti-soiling coating [3], with no anti-reflective performance [2]). The greatest *Difference* is observed for materials E and D (anti-reflective coatings, composed of porous silica [2], [3]). A green dashed line is shown relative to the *Actual* $\Delta\tau_h$ to indicate the change in performance if the coating was removed from unsoiled B, D, E, or U specimens.

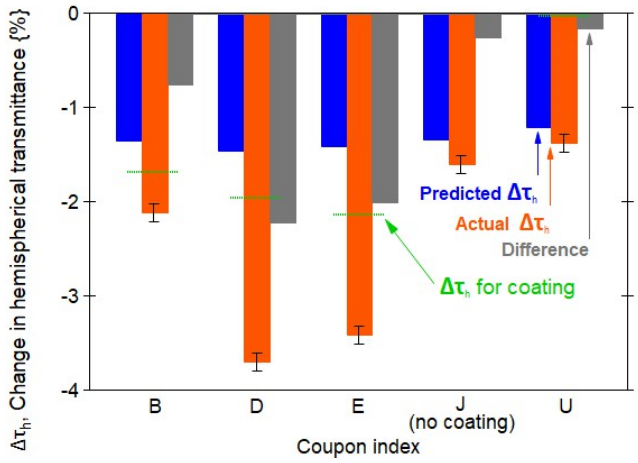

Fig. 1. Change in hemispherical transmittance for dry-brush-cleaned specimens after 1 year in Dubai. The *Predicted* $\Delta\tau_h$, measured *Actual* $\Delta\tau_h$, and their *Difference* (*Actual* $\Delta\tau_h$ minus *Predicted* $\Delta\tau_h$) are shown. The $\Delta\tau_h$ *for coating* (relative to unaged substrate glass) is indicated relative to the *Actual* $\Delta\tau_h$ with a green dashed line.

Regarding the *Actual* $\Delta\tau_h$ in Fig. 1, it was found to consistently exceed $\Delta\tau_h$ *for coating*. This suggests that contamination alone cannot account for the loss of transmittance. Abrasion during cleaning could account for the *Difference* in Fig. 1, e.g., if the coating has been damaged and/or removed by the DB cleaning. Heterogeneity of contamination could contribute towards the *Difference*, but the extent is expected to be limited because: (a) a greater uniformity of contamination was qualitatively observed for cleaned specimens (including dry brush), (b) at least five separate test locations were examined on each specimen to quantify PAC, (c) at least three separate test locations were examined on each specimen to quantify τ_h, and (d) the spot size of 1 cm 1 x cm was used to quantify τ_h (averaging the effect of variation). Damage including scratches through the thickness of the coating was previously observed [3]. While extensive damage was observed for many of the specimens fielded in Dubai, the most damaging location, the coating was not completely removed for many of the coupons. The *Actual* $\Delta\tau_h$, exceeding the $\Delta\tau_h$ *for coating*, may indicate additional optical interactions, including optical scattering (at contamination or scratches), absorption (e.g., from contamination within scratches, the accumulation of a thin cemented surface layer), and/or the limitations of the simple model for *Predicted* $\Delta\tau_h$ from the PAC. The relative contribution of the aforementioned optical interactions is not quantified here but it left for a future study.

3.2 Characteristics of the field contamination and abrasion

Table I summarizes the characteristics of the NC samples from the outdoor locations, including: PSD {μm}; PAC {%}; and $C_{soiling}$, the mass concentration, {g·m^{-2}}. The PSD is also given in the table for the ISO 12103-1 AZ test dust, from the vendor's lot inspection data. The size of particles did not vary greatly between the outdoor locations at the 5th or 50th percentile of the cumulative distribution but varied more at the 95th percentile. The largest PSD (greatest size at the 95 percentile) was observed for the specimens fielded in Dubai and Mesa. The majority of the A4 dust (used in the artificial abrasion experiments) exceeds the 95th percentile of the PSD of the NC field coupons. A PAC less than 10% (50th percentile) was observed for Kuwait City, Mesa, Mumbai, and Sacramento. A greater PAC, which varied between samples by ±~10%, was observed for Dubai. The largest average and maximum $C_{soiling}$ values were observed for Dubai.

Regarding Table I, the PSD is most varied at the 95th percentile, suggesting the effect of individual large particles. From PSD and PAC, Dubai and Mesa had the largest particles, possibly enhanced by the process of cementation [7]. Water spotting was observed for all NC specimens, consistent with the process of cementation. The variable PAC and $C_{soiling}$ give a sense of the localized nature of the contamination, which may vary noticeably within the same specimen. The sample area for Table I (using the VHX-5000 microscope) is less than that in Fig. 1 (using the Cary 5000 spectrophotometer), making the table more prone to localized variation.

TABLE I: SUMMARY OF PARTICLE SIZE DISTRIBUTION, PARTICLE AREA COVERAGE, AND MASS CONCENTRATION FOR FIELD COUPONS AFTER 1 YEAR AND AZ TEST DUST USED IN THIS STUDY.

SAMPLE	PSD (5th-**50th**-95th PERCENTILE) {μm}	PAC (MIN-**AVG**-MAX) {%}	$C_{soiling}$ (MIN-**AVG**-MAX) {g·m^{-2}}
Dubai	1.5-**2.3**-12.1	8.4-**23.0**-31.7	1.9-**9.5**-17.6
Kuwait City	1.1-**2.4**-8.0	4.7-**8.6**-15.3	1.0-**1.8**-3.4
Mesa	1.1-**2.8**-11.9	4.2-**5.3**-6.2	1.2-**1.6**-2.5
Mumbai	1.1-**2.4**-8.4	2.0-**4.1**-6.3	0.5-**1.0**-1.8
Sacramento	1.1-**2.2**-7.3	1.4-**2.3**-3.7	0.4-**0.7**-1.1
ISO 12103 A1	1.0-**4.5**-9.5	N/A	N/A
ISO 12103 A2	1.0-**8.0**-59	N/A	N/A
ISO 12103 A3	1.6-**14.2**-85	N/A	N/A
ISO 12103 A4	2.4-**34.2**-140	N/A	N/A

The morphology of scratches on the surface of DB-cleaned specimens after 1 year in Dubai is summarized in Table II. Parameters in the table include: w_s, the scratch width {μm}; h_s, the scratch depth {nm}, and h_n, the nominal coating thickness {nm}. The minimum, average (in boldface), and maximum values are given from the AFM measurements in Table II for w_s, and h_s. Representative values from ellipsometry are given for h_n in Table II to give a sense of the order of magnitude of the coating thickness. In the table, w_s was found to vary from micrometers to tens of micrometers. In Table II, h_s was found to vary from tens to hundreds of nanometers. For coupons B, D, and E, h_s did not always extend through the entire thickness of the coating. The minimum h_s was observed for the J specimens with no coating. The scratches had a linear shape, with a length at least in the order of tens of micrometers.

Regarding Table II, w_s was found to be at least an order of magnitude less than the size of bristles used in the experiment. w_s was, however, found to be comparable to the size of the contamination present on the surface of the coupons. This identifies that the surface damage results from the contamination, which acts as a localized abrasive when dragged across the surface by brush bristles. The scratches in the J coupons (consisting of just glass substrate, with no coating) identify the damage that may occur from the direct abrasion of the glass substrate. Scratches in the U coating were observed to extend a commensurate amount at other field sites, i.e., deeper than the nominal thickness of the coating. U is the only polymer coating in Table II. Local deformation of the U coating (including inelastic stretching of the polymer) at the edges of scratches may exaggerate the h_s values in the table.

TABLE II: MEASURED SCRATCH GEOMETRY FOR THE DRY-BRUSH-CLEANED SPECIMENS AFTER 1 YEAR IN DUBAI. MINIMUM, **AVERAGE**, AND MAXIMUM VALUES ARE PROVIDED.

COUPON INDEX	w_s, SCRATCH WIDTH {μm}	h_s, SCRATCH DEPTH {nm}	h_n, NOMINAL COATING THICKNESS {nm}
B	5.1-**7.3**-11.7	38-**105**-137	125
D	4.7-**16.9**-34.2	40-**64**-74	140
E	3.1-**12.7**-27.4	6-**94**-130	130
J	0.6-**9.3**-34.8	23-**37**-60	0 (no coating)
U	0.6-**1.5**-2.3	33-**106**-170	25

3.3 Characteristics of the artificial machine abrasion

The characteristics of the brush bristles used in this study are summarized in Table III, including the glass- and phase-transition temperatures as well as the diameter (for unused bristles). The table distinguishes the bristle materials used in the artificial and field coupon experiments. The glass-transition temperature, T_g or T_α, is given as the average value from heating and subsequent cooling. The melt- and freeze-transition temperature, T_m or T_f, are given from a single pass, i.e., the final heating or cooling of the specimen. Nylon and polyester have multiple melt and freeze transitions; the transition with the greatest enthalpy is given first for T_m and T_f. Instances where no transition was found are indicated as "N/A." Polyester is not a standard material for the brush vendor; the larger diameter is shown for the material used in artificial abrasion study.

TABLE III: BRUSH BRISTLE CHARACTERISTICS, INCLUDING GLASS- AND PHASE-TRANSITION TEMPERATURES AS WELL AS PHYSICAL DIMENSIONS.

BRISTLE MATERIAL: COMPOSITION	ABRASION EXPERIMENT	$T_{g1}=T_{\alpha1}$ {°C}	T_{c1} {°C}	T_{c2} {°C}	T_{m1} {°C}	T_{m2} {°C}	BRISTLE DIAMETER {mm}
Nylon 6/12	artifical	125	188	162	215	200	0.30
hog bristle	artifical	176	N/A	N/A	N/A	N/A	0.22
polyester	artifical	106	196	N/A	224	215	0.64
horsehair	field	153	N/A	N/A	N/A	N/A	0.25

Hog bristle and horsehair only exhibit a T_g in Table III. While it was not verified in this study, presumably the hog bristle and horsehair will undergo thermal decomposition at temperatures greater than 250 °C as identified in Ref. [9]. Nylon and polyester both exhibit a glass transition, along with multiple melt and freeze transitions. The transition temperatures in Table III exceed the nominal maximum operating temperature for a PV module, which may range up to 108 °C for building-integrated PV in a desert climate [8]. The diameter for the polyester in Table III, which exceeds the size of bristles in commercial brushes, will result in a greater stiffness for that material (as bending stiffness of a cantilever beam is proportional to the 4th power of the diameter [9]).

The materials typically used for brush bristles were also explored with the artificial abrasion study, including the purchase of representative brushes marketed to the PV industry. Bristle materials may generally be classified as Nylon, hog bristle, or synthetic. Nylon is the hardest material, giving it a slow wear rate and corresponding low cost of use when amortized through its life [9]. Nylon is also the easiest bristle material to clean, also providing low cost of use. Nylon 6 swells more with water, and therefore, it may fatigue faster than Nylon 6/12 [9]. Hog bristle is a natural material, obtained from along the spine of a boar's back. Hog bristle comes at a premium price, but it is preferred in the automotive industry because of its reduced propensity to scratch clearcoat paint systems. Hog bristle is not commonly used in the MENA region for religious and cultural reasons. Other synthetic materials include polyester, polystyrene, and polypropylene. These bristles are made from resins with a lower cost than Nylon. The synthetic materials are softer than Nylon, resulting in a faster wear rate. Of the brushes purchased, the bristle diameter was found to vary between 0.25 mm and 0.50 mm, with the length ranging from 3.1 cm to 7.5 cm. Of the brushes purchased, not all were found to contain bristles made of the same material identified in product catalogs. For example, polyester or a blend of Nylon and polyester (verified) were used instead of pure Nylon (catalog).

The effect of artificial abrasion as a function of n, the cycle count {dimensionless}, is shown in Fig. 2. Optical *haze*, which

varies with τ_h and τ_d, is defined in the figure. Decrease in hemispherical transmittance, τ_h, and increase in *haze* with the number of cycles, *n*, are both generally observed in the figure. The greatest decrease in τ_h is seen for the Nylon brush. The brushes are more readily distinguished by their *haze*, which results from the effect of optical scattering. For *haze*, much of the damage to the glass specimen occurs after 10000 brush cycles. The hog bristle brush is the least damaging in Fig. 2, with minimal change in *haze*.

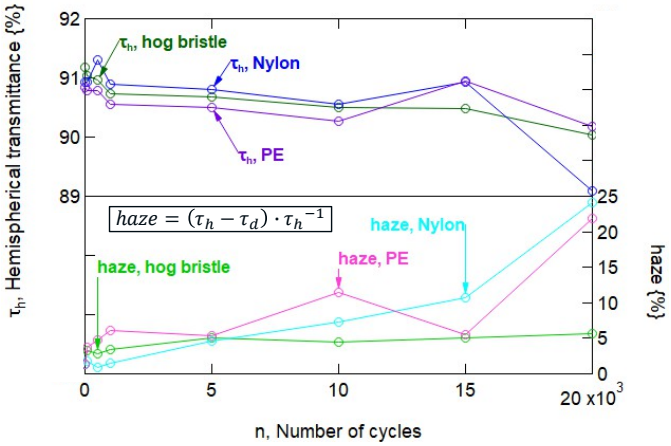

Fig. 2. Hemispherical transmittance and *haze* as a function of the number of dry-brush cycles for J glass (no coating).

The initial decrease in τ_h in the order of tenths of a percent in Fig. 2 is consistent with the *Difference* in Fig. 1, where the field coupons have been brush-cleaned 12 times. As in Fig. 1, however, the initial decrease in Fig. 2 may result from optical scattering (at scratches or remaining test dust), absorption (e.g., from contamination within scratches, the accumulation of a thin cemented surface layer). Fig. 2 identifies that although not examined in the field coupon study, the bristle material can affect the abrasion damage in addition to the abrasive, i.e., the surface contamination. Nylon is known to be the hardest and most mechanically stiff of the bristle materials examined in Fig. 2 [9]; therefore, the greatest final *haze* is expected for that material. The latent increase in *haze* (occurring after thousands of brush cycles) suggests that glass with no coating can be cleaned many times (e.g., over years) before the performance of a PV module is affected. The degradation of a coating on glass, however, may occur at a different rate than in the artificial abrasion experiments. The abrasion of glass in Fig. 2 provides a baseline that can be subsequently referenced during the abrasion testing of coatings.

The variation in surface roughness and surface energy (contact angle) with artificial abrasion as a function of *n* is shown in Fig. 3. The average surface roughness, R_a, increases from its initial value of 3.8 nm for all bristle materials. A much greater increase in roughness is seen for Nylon and polyester, including an undulation at 15000 cycles. The contact angle, *CA*, is seen to immediately decrease (the surface energy is correspondingly increased) from its initial value of 43° for "hydrophilic" [2] glass. The contact angle remains decreased for hog bristle. A more complex *CA* history is seen for Nylon and polyester, including a gradual increase in *CA* at 1000 followed by a peak at 15000 cycles. Similar complex behavior for transmittance, R_a, and *CA* was observed for replicate specimens at 15000 and 20000 cycles.

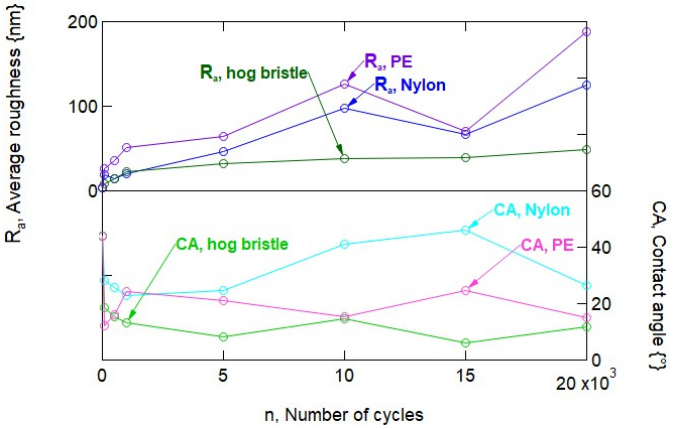

Fig. 3. Surface roughness and surface energy as a function of the number of dry-brush cycles for J glass (no coating).

The general trend of increased R_a with *n* is consistent with the increased scratching of the surface. A corresponding loss of τ_h and increased *haze* would therefore be expected with *n* based on the increased surface roughness. The subsequent variation in *CA* with *n* for Nylon and polyester was unexpected. The anticorrelation between R_a and *CA* might be explained by the deposition of dust onto the glass with abrasion cycles or the deposition of the residual bristle material through the experiments. The method of tribologically induced deposition has been used for thin films based on the locally elevated temperature at bristle tips [10]. The steady-state temperature of ~55 °C was observed in prolonged thermocouple and thermography measurements of the coupon surface for the Nylon brush. The local temperature at the bristle tips likely exceeds their global temperature. Local electrostatic discharge in dry conditions may also contribute to the evolution of τ_h, *haze*, R_a, and *CA*.

The morphology of scratches on the surface of the artificial abrasion specimens is summarized in Table IV. Parameters in the table include: *n*, the number of cycles (100 or 20000); w_s, the scratch width {μm}; and h_s, the scratch depth {nm}. The minimum, average (in boldface), and maximum values are given from the AFM measurements in Table IV for w_s and h_s. The average w_s increases from 1–2 μm at 100 cycles to 2–10 μm at 20000 cycles. In comparison, the average w_s of 9.3 μm was observed in Table II for the J (no coating) DB-cleaned field coupon specimens. In Table IV, the average h_s increases from 70–140 nm at 100 cycles to 200–800 nm at 20000 cycles. In comparison, the average h_s of 40 nm was observed in Table II for the J field coupon specimens. The maximum h_s values at 100 cycles in Table IV correspond to large individual scratches observed on the specimens, observed in addition to more numerous subtle scratches. The maximum w_s and h_s values at 20000 cycles in Table IV correspond to multiple individual scratches for the Nylon and polyester bristles, where 2–4

similar-sized scratches were often observed in the same measurement. The size of the scratches for the polyester bristles were difficult to identify because a single flat surface could not be identified throughout the AFM scans. The w_s and h_s given, however, provide a sense of the order of magnitude of the size of the rounded scratches observed on that coupon.

TABLE IV: MEASURED SCRATCH GEOMETRY FOR J (NO COATING) GLASS COUPONS IN THE ARTIFICIAL ABRASION EXPERIMENTS. MINIMUM, **AVERAGE**, AND MAXIMUM VALUES ARE GIVEN.

BRISTLE MATERIAL	n, NUMBER CYCLES	w_s, SCRATCH WIDTH {µm}	h_s, SCRATCH DEPTH {nm}
Nylon 6/12	100	0.8-**1.9**-4.5	30-**69**-154
hog bristle	100	0.8-**1.3**-2.0	25-**96**-256
polyester	100	0.6-**1.6**-5.0	22-**139**-552
Nylon 6/12	20,000	1.9-**5.8**-14.8	192-**325**-632
hog bristle	20,000	0.8-**2.1**-6.7	43-**202**-387
polyester	20,000	6.5-**11**-16	245-**802**-1700

Several factors may contribute to the differences between the morphology of the artificial and field coupon specimens, including: 1) use of coatings, 2) n used in the experiments, 3) particle size, 4) bristle geometry, 5) bristle material, and 6) accumulation of a surface layer. In 1), while most specimens in Table II are coated, all specimens in Table IV are composed of glass with no coating (index J in Table II). The coatings in Table II consist of porous or polymer materials, expected to have a hardness and mechanical modulus less than that of glass. The greater average w_s in Table II may result from the greater susceptibility of the coatings to abrasion damage. In 2), the greater h_s in Table IV at n = 100 reflects the occurrence of individual larger scratches (an average h_s in the order of 70 nm is observed if the larger scratches are censored). A greater h_s might be expected for Table IV (where n = 100) relative to Table II (where n = 12), as a greater n may facilitate more abrasion damage. For 3), in Table II, the particle size for A4 test dust (used in the artificial abrasion study) exceeds that of the size of the particles remaining on the field coupons. The larger particle size used in the artificial abrasion study may facilitate greater w_s, and h_s. For 4), in Table III, the diameter of the horsehair in the field study is slightly bigger than the diameter of the hog bristle used in the artificial abrasion study. Assuming a round cantilever beam geometry, the ratio of 1.7 is obtained for the bending stiffness of the natural bristle materials, i.e., horsehair:hog bristle. The bristle length of 4.3 cm (horsehair) and 3.8 cm (hog bristle) was also different between the studies. Assuming a round cantilever beam geometry, the ratio of 0.70 is obtained for the bending stiffness of the natural bristle materials, i.e., horsehair:hog bristle. The factors of bristle diameter and length mostly cancel out when considered together, giving a stiffness ratio of 1.2, i.e., horsehair:hog bristle. In 5), hog bristle and horsehair are both classified as keratins, which should give similar hardness and mechanical modulus. The hardness and modulus of keratins are less than that of Nylon and polyester, giving the natural bristle materials a greater compliance and reducing their contribution to abrasion damage. In 6), the large scratches observed in Table IV at n = 20,000 may indicate the tribological deposition of a thin film of contamination on the specimen surface. The w_s and h_s do not exceed the particle size of the A4 abrasive used in the experiments for the Nylon and polyester bristles; however, large scratches may be more readily formed in a thin film of contamination than in the glass substrate. Evidence of a thin film of contamination on glass coupons was observed in discovery experiments comparing dry- and slurry-brush abrasion [11]. Microscopy and chemical analysis will be used to further assess the specimens in this study.

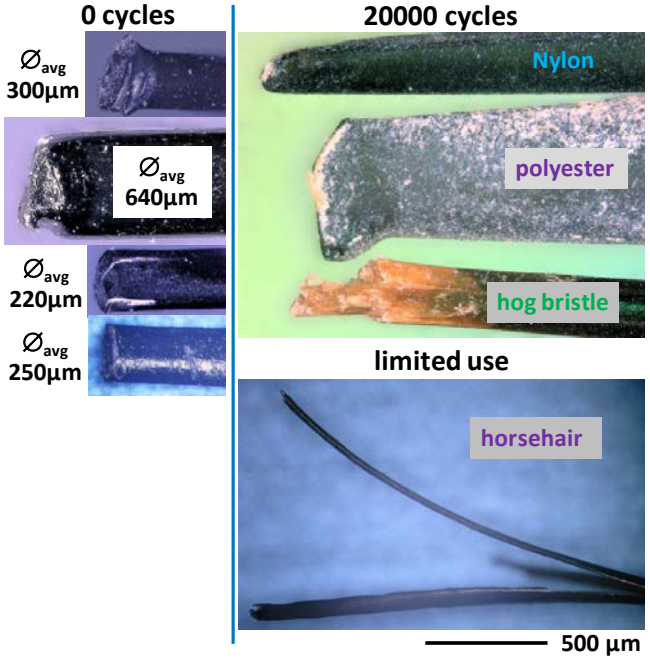

Fig. 4: Tip geometry and bristle size for the artificial abrasion experiments. Unused bristles (left) are compared to bristles after 20000 cycles of dry abrasion with ISO 12103-1 A4 test dust or limited use (right).

The tip geometry and bristle size are compared in representative images in Fig. 4. Unused bristles are compared in Fig. 4 (left) to bristles after 20000 cycles or limited use, Fig. 4 (right). As shown in Fig. 4 (left), the horsehair bristles were cut to length prior to the start of the field coupon study. The Nylon tip is rounded, with a tapered diameter after 20000 cycles, Fig. 4 (right). The PE tip is flattened, and the size of its end increased after 20000 cycles, Fig. 4 (right). The used hog bristle tip has an irregular shape, including a flared end. After limited use (~100 cycles from the as-received condition), the horsehair tip is split at its end, which was typical for bristles from the brush. The bristle diameter for brushes used for cleaning the field coupons ranged from 154-**246**-335 µm in Fig. 4 (left), being statistically different than the diameter of the split ends represented in Fig. 4 (right) that ranged from 13-

39-180 μm, i.e., for 5%-**50**%-95% of the cumulative distribution.

The blunted PE and rounded Nylon tips in Fig. 4 are consistent with the occurrence of phase transitions for those materials in Table III. The rounded Nylon tip may also suggest wear from abrasion. The irregular shape for the hog bristle tip corresponds to a material that does not melt but may physically wear or decompose at elevated temperature. Likewise, the split ends observed for the horsehair bristles suggest mechanical damage rather than a phase transition. The tip shape was examined in Fig. 4 for dry brush abrasion only.

IV. Discussion

The PSD of the NC field specimens as well the damage morphology of the DB field specimens may be compared to the artificial abrasion specimens to assess the abrasive used in accelerated tests. The size of airborne particulate contamination is known to exceed that in Table I [12]. Furthermore, the median size of 15 μm was observed in a review of the literature examining the contamination of the surface of PV modules [15]. In contrast, the median size of ~2.5 μm is observed in Table I for the contamination in the field coupon study. The particle sizes in Table I are also less than those recently reported by the collaborators at some of the field sites used in this study [13,14]. The maximum size of the contamination in Table I is likely limited not only by natural cleaning (the extent of wind and precipitation and their recentness relative to collecting the specimens from the field sites) but also by the handling of the specimens during return shipment. For example, consider the maximum width of scratches observed in Table II (that ranges up to 35 μm) relative to the PSD of the field coupons in Table I (that ranges up to 12 μm). The PSD of the NC specimens in Table I is believed to underestimate the size of contamination found on a field soiled module.

The similar size of the scratches in Table II and Table IV, reminds that the abrasive is a primary factor affecting the abrasion damage. While the scratches in the field coupon study are often wider and the scratches in the artificial abrasion study are often deeper, w_s and h_s are similar in Table II and Table IV, being within the same order of magnitude. In contrast, the diameter of the bristles is more than an order of magnitude larger than the w_s and h_s of the scratches, including the coated field coupons. The similar size of the scratches in Table II and Table IV might be unexpected, considering the relatively large size of the A4 test dust used in the artificial abrasion study, which exceeds the size of the contamination observed on the field coupons. While not actively examined in this study, the size and shape of the contamination may affect surface abrasion. An abrasive similar in size to that encountered in the field is recommended to achieve a representative abrasive behavior in artificial abrasion tests. While it could not be corroborated in the field coupon study, the A2 test dust is recommended to give a PSD intermediate to the field coupon study and the literature [15].

The composition of the abrasive is also anticipated to be a significant contributor to surface abrasion. While not examined in this study, the composition of soil and airborne particulate matter is known to vary with location [16]. Compared with the Sahara, Gobi, and Mojave deserts, the Middle East was found to contain lower proportions of SiO_2 and higher proportions of CaO (much softer than glass) and MgO (hardness greater than glass). The hardness of the contamination will affect the rate of abrasive damage. Palygorskite is a mineral commonly found in MENA locations and the southeastern USA, but not in AZ. Clays and salts may interact and cement to the surface, affecting the rate of abrasive damage. Because AZ test dust has important chemical differences relative to other locations, the identification and use of additional dusts is recommended for future abrasion studies.

The change in optical performance, surface-roughness, and surface-energy in Fig. 2 and Fig. 3 identify that the secondary effects of the bristle material must also be considered in PV abrasion. The immediate increase in surface energy, enhancing hydrophilicity, may result from cleaning of the surface. In comparison, a pumice scrub may be used to clean glass of industrial chemicals and/or organic contamination during PV fabrication [17]. Bristle-specific effects become manifest in Fig. 2 and Fig. 3 at 10000 cycles. Effects at n>10000 correspond to a product lifetime in the order of ~14 years, assuming the module surface is swiped once daily in forward and reverse directions. The results in this study imply that a natural fiber bristle may be used to reduce surface damage in PV installations where daily cleaning is required. Regarding accelerated testing for the purposes of material selection or design qualification, the bristle-specific results in Fig. 2 and Fig. 3 confirm the importance of standardizing the bristle material and bristle geometry to facilitate the comparison of results between different coatings, substrate materials, and laboratories. While longer bristles are used in the PV industry, 3.8 cm long bristles may be used in 5060 linear brush tester, which will give some acceleration of the artificial abrasion relative to cleaning for operations & maintenance. The bristle material Nylon 6/12 is recommended for standardization based on its popular use in the PV industry as well as the present trend toward its use in abrasion test standards in other industries. Regarding natural and artificial abrasion, the rate of abrasion of surface coatings may vary from the monolithic glass specimens examined in this study.

The distinctions between the bristle materials in Fig. 2 and Fig. 3 generally correlate with the known use of those materials. The natural material (i.e., hog bristle) least affected the glass surface, consistent with its popular use in the automotive industry. The mechanical characteristics (lesser hardness and modulus [9]) as well as the behavior at elevated temperature (favoring thermal decomposition) likely contribute to the distinctions observed for hog bristle in Fig. 2 and Fig. 3. The synthetic bristle materials (more often used in

the building glazing industry) more greatly affected the glass specimens. The more complex evolution of optical performance, surface roughness, and surface energy may result from interaction between the brush, abrasive, and specimen, including the melting of the bristle material and tribological deposition of a thin film of contamination. For the dry brush test it is unclear if melted bristle material (for Nylon 6/12 or polyester) may interact with substrate and/or dust. Significant differences may also exist between the dry-brush abrasion in Fig. 2 and Fig. 3 and a slurry abrasion study, because water may act as a lubricant and coolant, especially in low cycle counts. The study here focuses on "recently" soiled specimens, whereas the abrasion of soiled specimens with subsequent cementation may occur at a different rate with different characteristics.

V. Summary

This study examines the abrasion of photovoltaic coatings and glass, including both field coupon and artificial abrasion experiments. Key results include the following:

The optical transmittance of field coupon specimens after one year (12 cleanings) was reduced in excess of that predicted from the particle area coverage of contamination as well as the performance of anti-reflective surface coatings, identifying the effects of abrasion damage. The further study of abrasion (including the comparison of the final damage morphology) is recommended in addition to the development of an abrasion test standard tailored to PV.

The size of the contamination remaining on the field coupon specimens was found to range from 1 μm to 12 μm. "Fine" A2 ISO 12103-1 AZ test dust is recommended as an artificial abrasive in accelerated tests to account for adhered contamination as well as contamination that may have been removed by natural cleaning and/or specimen transportation.

The similar size of the scratches in the field coupon study and the artificial abrasion study highlights that the surface contamination is a primary factor affecting the abrasion damage. The use of additional dusts (to be determined) is recommended to give representative artificial surface abrasion tailored to other world locations.

Brush bristle materials were distinguished in an artificial abrasion experiment, at the cycle count of 10000. A single bristle material (Nylon 6/12) and bristle geometry is therefore recommended for the standardization of artificial abrasion.

Acknowledgement

The authors would like to thank Telia Curtis, Sai Ravi Vasista Tatapudi, and Professor Govindasamy Tamizhmani of Arizona State University; Pedro Banda, Ammar Elnosh, and Marco Stefancich of Dubai Electricity and Water Authority; Vasi Juzer, Sonali Warade, and Professor Anil Kottantharayil of the Indian Institute of Technology Bombay; Bader Alabdulrazzaq, Ayman Al-Qattan, and Feras Al-Zubi of Kuwait Institute for Scientific Research; and Michael Anderson, Ben Bourne, Zoe Defreitas, Fabrizio Farina, Greg Kimball, and Jorge Zuniga of the SunPower Corporation for their help with the outdoor field coupon study. This work was supported by the U.S. Department of Energy (DOE) under Contract No. DE-AC36-08GO28308 with Alliance for Sustainable Energy, LLC, the Manager and Operator of the National Renewable Energy Laboratory (NREL). NREL is a national laboratory of the DOE, Office of Energy Efficiency and Renewable Energy. The views expressed in the article do not necessarily represent the views of the DOE or the U.S. Government. Instruments and materials are identified in this paper to describe the experiments. In no case does such identification imply recommendation or endorsement by NREL. The U.S. Government retains and the publisher, by accepting the article for publication, acknowledges that the U.S. Government retains a nonexclusive, paid-up, irrevocable, worldwide license to publish or reproduce the published form of this work, or allow others to do so, for U.S. Government purposes.

References

1. T. Sarver, A. Al-Qaraghuli, and L. L. Kazmerski, "A comprehensive review of the impact of dust on the use of solar energy: History, investigations, results, literature, and mitigation approaches," Renew. Sust. Energ. Rev., vol. 22, pp. 698–733, 2013.
2. S. Toth, M. Muller, D. C. Miller, H. Moutinho, B. To, L. Micheli, J. Linger, C. Engtrakul, A. Einhorn, and L. Simpson, "PV soiling and cleaning: Initial observations from 5-year photovoltaic glass coating durability study," Sol. Energ. Mat. Sol. C, pp. 375–384, 2018.
3. A. Einhorn, L. Micheli, D.C. Miller, L.J. Simpson, H.R. Moutinho, B. To, C.L. Lanaghan, M.T. Muller, S. Toth, J.J. John, S. Warade, A. Kottantharayil, C. Engtrakul, "Evaluation of Soiling and Potential Mitigation Approaches on Photovoltaic Glass," J. Photovolt., 2018, 9(1), 2018, 233–239.
4. "ISO 12103-1: Road vehicles – Test contaminants for filter evaluation – Part 1: Arizona test dust," International Standards Organization: Geneva, 2016, pp. 1–14.
5. "ISO 13322-1: Particle size analysis – Image analysis methods – Part 1: Static image analysis methods," International Standards Organization: Geneva, 2014, pp. 1–24.
6. D.C. Miller, J. Apezteguia, J.G. Bokria, M. Köhl, N.E. Powell, M.E. Smith, M.D. White, H.R. Wilson, J.H. Wohlgemuth, "Examination of an Optical Transmittance Test for Photovoltaic Encapsulation Materials," Proc SPIE, 2013, 8825-8.
7. C.L. Perkins, M. Muller, L. Simpson, "Laboratory Studies of Particle Cementation and PV module Soiling," Proc. IEEE PVSC, 2017, 2294–2297.
8. D.C. Miller, M.D. Kempe, S.H. Glick, S.R. Kurtz, "Creep in Photovoltaic Modules: Examining the Stability of Polymeric Materials and Components," Proc. IEEE PVSC, 2010, 262–268.
9. "Filament Performance in Brushes," white paper, E. I. du Pont de Nemours and Co., 2014, 1–31.
10. J.O. Aguilar, J.M Rodríguez-Lelis, M.J. Arjona, "Iron oxide coating films in soda-lime glass by triboadhesion," J. Mech. Sci. Technol., 23, 2009, 1169–1174.

11. C.L. Perkins, H. Moutinho, C.-S. Jiang, L. Simpson, "Surface chemistry of PV module glass: implications for module soiling," Proc. Int. Soiling Work., 2018.
12. W.E. Wilson, H.H. Suh, "Fine Particles and Coarse Particles: Concentration Relationships Relevant to Epidemiologic Studies," J. Air Waste Manage. Assoc., 47, 1997, 1238–1249.
13. J.J. John, S. Warade, G. Tamizhmani, A. Kottantharayil, "Study of soiling loss on photovoltaic modules with artificially deposited dust of different gravimetric densities and compositions collected from different locations in India", IEEE J PV, 6 (1), 2016, 236-243.
14. A. Alnuaimi, J. John, O. Albadwawi, Y. Elhassan, F. Albanna, F. Almamari, A. Alqassim, "Quantification of spectral losses of Natural soiling and detailed microstructural analysis of Dust collected from Different locations in Dubai, UAE", Proc IEEE PVSC Conf., 2019, xxx.
15. I. Nayshevsky, Q.F. Xu, A. Lyons, "Literature Survey of Dust Particle Dimensions on Soiled Solar Panel Modules," Proc. Intl Soiling Work., 2018.
16. J.P. Engelbrecht, E.V. McDonald, J.A. Gillies, R.K.M. Jayanty, G. Casuccio, A.W. Gertler, "Characterizing Mineral Dusts and Other Aerosols from the Middle East—Part 1: Ambient Sampling," Inhalation Toxicology, 21, 2009, 297–326.
17. D.C. Miller, M.D. Kempe, C.E. Kennedy, S.R. Kurtz, “Analysis of Transmitted Optical Spectrum Enabling Accelerated Testing of Multi-Junction CPV Designs,” Opt. Eng., 50(1), 2011, 013003.

TABLES:

TABLE I: SUMMARY OF PARTICLE SIZE DISTRIBUTION, PARTICLE AREA COVERAGE, AND MASS CONCENTRATION FOR FIELD COUPONS AFTER 1 YEAR AND AZ TEST DUST USED IN THIS STUDY.

SAMPLE	PSD (5th-**50th**-95th PERCENTILE) {μm}	PAC (MIN-**AVG**-MAX) {%}	$C_{soiling}$ (MIN-**AVG**-MAX) {g·m^{-2}}
Dubai	1.5-**2.3**-12.1	8.4-**23.0**-31.7	1.9-**9.5**-17.6
Kuwait City	1.1-**2.4**-8.0	4.7-**8.6**-15.3	1.0-**1.8**-3.4
Mesa	1.1-**2.8**-11.9	4.2-**5.3**-6.2	1.2-**1.6**-2.5
Mumbai	1.1-**2.4**-8.4	2.0-**4.1**-6.3	0.5-**1.0**-1.8
Sacramento	1.1-**2.2**-7.3	1.4-**2.3**-3.7	0.4-**0.7**-1.1
ISO 12103 A1	1.0-**4.5**-9.5	N/A	N/A
ISO 12103 A2	1.0-**8.0**-59	N/A	N/A
ISO 12103 A3	1.6-**14.2**-85	N/A	N/A
ISO 12103 A4	2.4-**34.2**-140	N/A	N/A

TABLE II: MEASURED SCRATCH GEOMETRY FOR THE DRY-BRUSH-CLEANED SPECIMENS AFTER 1 YEAR IN DUBAI. MINIMUM, AVERAGE, AND MAXIMUM VALUES ARE PROVIDED.

COUPON INDEX	w_s, SCRATCH WIDTH {μm}	h_s, SCRATCH DEPTH {nm}	h_n, NOMINAL COATING THICKNESS {nm}
B	5.1-**7.3**-11.7	38-**105**-137	125
D	4.7-**16.9**-34.2	40-**64**-74	140
E	3.1-**12.7**-27.4	6-**94**-130	130
J	0.6-**9.3**-34.8	23-**37**-60	0 (no coating)
U	0.6-**1.5**-2.3	33-**106**-170	25

TABLE III: BRUSH BRISTLE CHARACTERISTICS, INCLUDING GLASS- AND PHASE-TRANSITION TEMPERATURES AS WELL AS PHYSICAL DIMENSIONS.

BRISTLE MATERIAL: COMPOSITION	ABRASION EXPERIMENT	T_{g1}=$T_{\alpha 1}$ {°C}	T_{c1} {°C}	T_{c2} {°C}	T_{m1} {°C}	T_{m2} {°C}	BRISTLE DIAMETER {mm}
Nylon 6/12	artifical	125	188	162	215	200	0.30
hog bristle	artifical	176	N/A	N/A	N/A	N/A	0.22
polyester	artifical	106	196	N/A	224	215	0.64
horsehair	field	153	N/A	N/A	N/A	N/A	0.25

TABLE IV: MEASURED SCRATCH GEOMETRY FOR J (NO COATING) GLASS COUPONS IN THE ARTIFICIAL ABRASION EXPERIMENTS. MINIMUM, AVERAGE, AND MAXIMUM VALUES ARE GIVEN.

BRISTLE MATERIAL	n, NUMBER CYCLES	w_s, SCRATCH WIDTH {μm}	h_s, SCRATCH DEPTH {nm}
Nylon 6/12	100	0.8-**1.9**-4.5	30-**69**-154
hog bristle	100	0.8-**1.3**-2.0	25-**96**-256
polyester	100	0.6-**1.6**-5.0	22-**139**-552
Nylon 6/12	20,000	1.9-**5.8**-14.8	192-**325**-632
hog bristle	20,000	0.8-**2.1**-6.7	43-**202**-387
polyester	20,000	6.5-**11**-16	245-**802**-1700